Unlocking the Potential of Battery Research

A New Expert Insight.
Download for free.

Battery research is essential to meet the growing demand for reliable, efficient, cost-effective energy storage solutions.

This expert insight presents recent research on solid polymer electrolytes (SPEs), recycling methods for lithium-ion batteries (LIBs), and cathode degradation during extreme fast charging (XFC) of electric vehicles.

PerkinElmer®
For the Better

WILEY

Received: 10 November 2021 | Revised: 2 April 2022 | Accepted: 17 April 2022

DOI: 10.1002/er.8030

RESEARCH ARTICLE

INTERNATIONAL JOURNAL OF ENERGY RESEARCH WILEY

Exploiting the synergistic catalytic effects of CoPi nanostructures on Zr-doped highly ordered TiO_2 nanotubes for efficient solar water oxidation

Maged N. Shaddad[1] | **Prabhakarn Arunachalam**[1] | **Mabrook S. Amer**[1,2] | **Abdullah M. Al-Mayouf**[1,2] | **Mahmoud Hezam**[3] | **Haneen A. AlOraij**[1] | **Sixto Gimenez**[4]

[1]Electrochemical Sciences Research Chair (ESRC), Chemistry Department, College of Science, King Saud University, Riyadh, Saudi Arabia

[2]Energy Research and Innovation Center at Riyadh, K.A.CARE, Riyadh, Saudi Arabia

[3]King Abdullah Institute for Nanotechnology, King Saud University, Riyadh, Saudi Arabia

[4]Institute of Advanced Materials (INAM), Universitat Jaume I, Castelló, Spain

Correspondence
Prabhakarn Arunachalam, Electrochemical Sciences Research Chair (ESRC), Chemistry Department, College of Science, King Saud University, Riyadh 11451, Saudi Arabia.
Email: parunachalam@ksu.edu.sa

Funding information
National Plan for Science, Technology, and Innovation (MAARIFAH), King Abdulaziz City for Science and Technology, Kingdom of Saudi Arabia, Grant/Award Number: 3-17-02-001-0011

Summary

Photoelectrochemical (PEC) catalysis offers promising strategies for sustainable development. This study demonstrated the synergistic catalytic behavior of ZrO_2 and a cobalt phosphate on anodized TiO_2 nanotubes (TNTs), which significantly enhanced the PEC performance for visible-light-driven water splitting reactions. The sequential addition of ZrO_2/CoPi-decorated TNTs was performed via electrodeposition and photoassisted electrodeposition. The substitution of Zr^{4+} by Ti^4 can lead to the creation of oxygen vacancies, enabling electron trapping, reducing charge recombination, and thereby enhancing the charge transfer efficiency. Further, in the case of TNTs/ZrO_2/CoPi photoanode, the CoPi WOC functioned as a hole-transfer relay to promote the water-splitting reaction. Specifically, incorporating ZrO_2/CoPi rushes the surface reaction kinetics of TNTs and considerably improves charge transfer efficiency (η_{CT} = 90%), photocurrent density (0.86 mA/cm^2 at 1.23 V_{RHE}) and durability were obtained. Further, the mechanistic examination by impedance measurements showed the enhanced charge transfer, and surface conductivity for prepared materials. The proposed method can be widely used to develop electrodes made of other materials to produce solar fuels.

KEYWORDS

cobalt phosphate, co-catalytic effect, surface engineering, TiO_2 nanotube bamboo structure, water splitting

1 | INTRODUCTION

The photoelectrochemical (PEC) water-splitting reaction induced by visible light offers ecological strategies to store energy in the bonds of H_2.[1] To proficiently implement the solar-fuel conversion, semiconducting materials that have suitable band energy levels, are likely to absorb a major part of the solar spectrum, and have low overpotentials for electrocatalytic reactions are mandatory. Extensive research has been conducted on PEC water splitting using numerous semiconductor photocatalysts since Fujishima and Honda's pioneering studies.[2] During the earlier stages of research, stoichiometric water splitting was not successful theoretically because of several difficulties, the simultaneous, reverse process, unstable nature of photocatalyst, poor variation in selecting photocatalyst and co-catalyst materials, etc. Over the past decade, exhaustive research has been performed to

achieve viable n-type semiconductors, as the oxygen evolution reaction is a kinetically more challenging reaction, and it involves severe oxidizing circumstances.[3,4] In this context, substantial research works have been executed to upsurge the efficiency of those solar-driven photocatalysts. Thermodynamically, converting water molecules into H_2 and O_2 is an energetically uphill t uphill reaction because it results in a significant change in Gibbs free energy. In order to efficiently transform solar photons into usable fuels, In order to achieve this, numerous metal oxide-based semiconductor photocatalysts have been extensively investigated (eg, TiO_2,[5,6] ZnO,[7,8] $SrTiO_3$,[9] Fe_2O_3,[10-12] and WO_3[13-15]). In this context, TiO_2 is considered to be a promising candidate for the PEC water-splitting reaction owing to its adequate band-edge levels, high optical stability, and high chemical inertness, and roubustness.[16-18] Besides, the wide-bandgap (≤3.2 eV) of undoped TiO_2 restricts its applications and confines its optical absorption to the UV part in the spectrum, leading to low PEC performance.[19] To boost conversion efficiency, the sensitization of TiO_2 with smaller-bandgap semiconductors,[12,20] as well as nonmetals and metal nanoparticles,[21,22] is regularly performed.

Since TiO_2 nanotubes (TNTs) were developed by Hoyer through a template-assisted process,[23] the influence of the fabrication aspects, doping methodologies, and applications of TNTs have been extensively investigated.[24-26] Highly oriented TNTs have been explored as photoanode materials owing to its high stability, high efficiency under UV light, and eco-friendly characteristics and have great potential for broad-spectrum energy absorption with low recombination.[27-29] In particular, TNTs provide great regulation over the separation of photoinduced charge carriers in PEC water-oxidation systems. A major advantage of TNTs is that this morphology can accommodate co-catalysts in the tube walls; that is, high spatial control of the co-catalysts can be achieved along the tube walls.[30-32]

In recent years, modifying photocatalytic materials with a water-oxidation catalyst (WOC) has been an appropriate pathway for promoting the PEC performance of TNTs as well as suppressing the recombination rate of carriers.[33] The recombination rate of excitons can be minimized via composite formation with WOCs, which function as electron and hole sink owing to their favorable band-edge positions.[34,35] In this context, cobalt phosphate (CoPi) complexes are excellent candidates for accelerating the water splitting reaction at a relatively lower bias.[36,37] Furthermore, these materials possess relatively high abundance levels, self-healing characteristics, and good effectiveness under benign circumstances. In recent years, CoPi complexes have been proved to function efficiently as WOC in electrocatalysis[38] and photoelectrocatalysis when integrated with ZnO,[39,40] Fe_2O_3,[11] WO_3,[41] $ZnTaO_2N$,[42] and $La(Ta,Nb)O_2N$[37] electrodes. Though it has not yet been fully specified, it is speculated that CoPi has a molecular structure involving edge-sharing CoO_6 octahedra[43] and a Co:P ratio of either 2:1 or 3:1.[38] During the oxidation of water, CoPi endures proton-coupled electron transfers as well as cyclic valency varies between Co(II/III) and Co(III/IV).[38] In photoelectrocatalysis, the fundamental function of CoPi is to suppress charge recombination by enhancing hole transport through the Co-ion valency cycle. Further, CoPi photostability under different composite materials was not studied in detail.

Electrochemical deposition is the most promising thin-film deposition technique in terms of scalability and ease of implementation. While, this method is restricted to depositing electrically conductive candidates, it can also be applied to incorporating co-catalytic materials over photoanodes with well-developed nanostructures. Using this solution-based process, morphology can be altered by varying the solution parameters, while altering the electrodeposition parameters can change the thickness, which are all controlled in ambient conditions. Because of this, this is a relatively cheap and practical method. We recently demonstrated a $BiVO_4$ photoanode with the controlled introduction of Zr and Fe precursors via electrodeposition and achieved an exceptional 4-fold enhancement for the PEC water-oxidation reaction. Moreover, ZrO_2 has also been introduced to passivate the $BiVO_4$ surface traps in PEC water oxidation.[44] Recently, we demonstrated that combining oxygen vacancies and metal doping of TNTs might effectively boost the efficiency of solar water splitting.[45] However, the synergistic combination of TNTs with WOCs and a surface passivation coating is an efficient strategy for enhancing the PEC water-splitting reactions.

Herein, we report heterostructured triple-layered TNTs/ZrO_2/CoPi photoanodes, which have high stability, are cost-effective and have not been investigated for the water-splitting system. In the photoanodes, the CoPi WOCs act as a hole-transfer relay to promote the water-oxidation kinetics; the ZrO_2 provides traps for charge carriers, preferring the spatial separation of charge pairs; and the TNT layer offers a pathway for electron transport. The fabricated TNTs/ZrO_2/CoPi photoanodes exhibited high PEC features for water oxidation, with a 3.5-fold increase compared with TNT photoanodes.

2 | EXPERIMENTAL SECTION

Ti foils (>99.5%, Alfa Aesar, 0.25 mm thickness) were used to fabricate TNTs. Ammonium fluoride (NH_4F) and

(Sigma-Aldrich, US), zirconium (IV) acetylacetonate ($C_{20}H_{28}O_8Zr$), cobalt nitrate hexahydrate ($Co(NO_3)_2{\cdot}6H_2O$), a phosphate buffer solution (PBS), and sodium sulfite (Na_2SO_3) were acquired from Sigma-Aldrich. Ethylene glycol (EG) was obtained from BDH.

2.1 | Fabrication of TNT arrays

TiO_2 NTs arrays were produced by electrochemical anodizing Ti foil at room temperature in two steps.[45] TNTs were ultrasonically cleaned and potentiostatically anodized for 30 minutes in an electrochemical system with a Pt foil counter electrode. The anodization process functioned at a continuous voltage of 60 V using NH_4F, water, and EG as the electrolyte solution. The Ti foil was removed and thoroughly cleaned with millipore water for a few seconds prior to the next potentiostat anodization step under similar conditions with a three-hour time delay. The anodized Ti foil was washed multiple times with millipore water before being annealed at 450°C for 120 minutes to produce crystalline TNTs over the foil.

2.2 | Fabrication of ZrO_2-decorated TNT electrodes

$TNTs/ZrO_2$ electrodes were fabricated via electrochemical deposition, using an electrodeposition bath containing a 5 mM Zr ($C_{20}H_{28}O_8Zr$) precursor in an EG solution. Typically, the electrochemical deposition was performed in a three-electrode assembly in an electrochemical system. The cathodic deposition was executed potentiostatically at −2.0 V vs Ag/AgCl with changing deposition times (2-15 s). The obtained electrode was then annealed at 450°C for 120 minutes in air.

2.3 | Fabrication of $TNTs/ZrO_2$/CoPi electrodes

WOC-CoPi was loaded on the $TNTs/ZrO_2$ photoanode via a photo-assisted electrochemical deposition process in a 0.1 M PBS enclosing 0.5×10^{-3} M cobalt nitrate under the 1.5G AM condition. Figure S1 shows the different phases of the synthesis method employed to acquire the triple-layered $TNTs/ZrO_2$/CoPi electrodes.

2.4 | Characterization of photoanodes

X-ray diffraction (XRD) analysis was performed via X-ray diffractometer (Rigaku Miniflex 600). The UV-visible diffuse reflectance spectra (DRS) were acquired via the Shimadzu UV-2600. The surface features of the fabricated photoanodes were inspected via scanning electron microscopes (JSM7600F, JEOL, Peabody, Massachusetts) attached to energy-dispersive X-ray spectrometers (EDS) and transmission electron microscopes (JEM 2100F, JEOL).

2.5 | PEC characterization

A PEC examination of the photoelectrodes was executed through cyclic voltammetry and electrochemical impedance spectroscopy (EIS) under irradiation (100 mW/cm^2) in a PBS solution with and without 1 M Na_2SO_3 as a hole scavenger. The classical three-electrode assembly comprised the working electrode, a reference electrode of Ag/AgCl and a counter electrode of Pt wire. Utilizing a thermopile, the light intensity was calibrated to 100 mW/cm^2. An incident photon-to-current efficiency (IPCE) analysis was performed using an Instytut Fotonowy.

The photoconversion efficiency (PCE) was estimated as follows:

$$\text{Photoconversion efficiency (PCE, \%)} = \frac{J_{PEC}(mA/cm^2) * (1.23 - V_{bias})V}{Pin(mW/cm^2)} \times 100, \quad (1)$$

where J_{PEC} represents the photocurrent density, V_{bias} represents the applied bias, and P_{in} represents the power density. The absorbed photon-to-current efficiency (APCE) spectra were estimated from the corresponding IPCE and light-harvesting efficiency spectra. Then, the APCE was assessed as follows:

$$APCE\,(\%) = \frac{IPCE}{LHE} \times 100. \quad (2)$$

3 | RESULTS AND DISCUSSION

3.1 | Microstructure and physicochemical properties of $TNTs/ZrO_2$ arrays

Figure 1 presents top-view and side-view SEM photographs of two-step anodized TNTs and $TNTs/ZrO_2$ films. As shown in Figures 1A to C, the obtained bare TNT arrays were well-ordered and uniformly arranged perpendicular to the substrate. From Figure 1B, the obvious parameters of the bare TNTs were as follows: tube diameters of 150 nm and an inner-wall thickness of

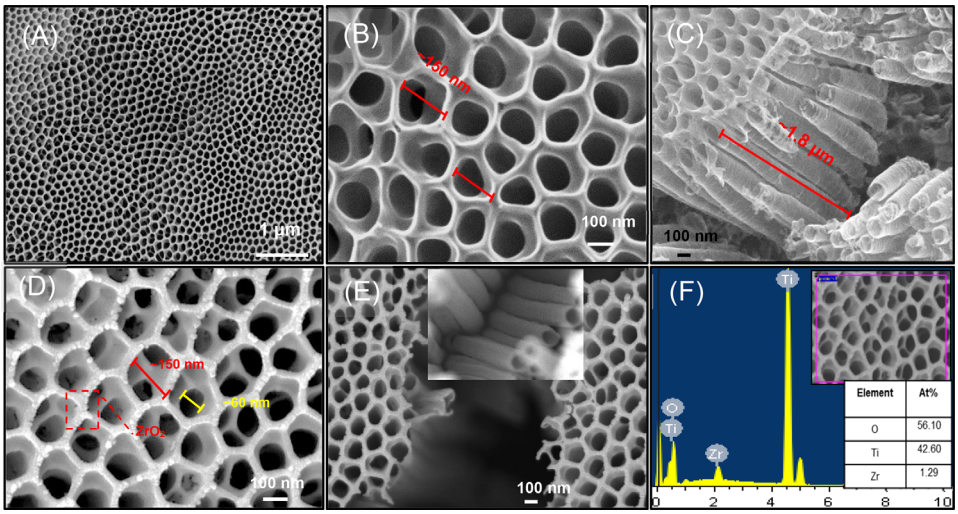

FIGURE 1 (A, B) FE-SEM images of TiO_2 nanotubes (TNTs) obtained via anodization process at 60 V for 1 hour and then removed via ultrasound followed by a second anodization procedure for 3 hours in an EG electrolyte with 0.1 M NH_4F and 0.5 vol% H_2O; (C) corresponding cross-section representation of the tubular morphology of the TNTs. (D, E) SEM images of TNTs loaded with ZrO_2 nanoparticles (2.5 mol%) deposited from a dimethyl sulfoxide solution (inset: cross-section). (F) Energy-dispersive X-ray spectrometers results for ZrO_2/TNTs

approximately 20 nm (Figure 1B). Additionally, characterization revealed that the bare TNTs had a smooth cross-section, with a nanotubes length of approximately 1.8 µm (Figure 1C). The optimized ZrO_2 nanoparticle films over TNT arrays fabricated via an electrodeposition process and the SEM photographs are presented in Figures 1D and E. Remarkable changes in the TNT surface morphology can be noticed after the decoration with ZrO_2, where the ZrO_2 particles were homogenously dispersed over the TNTs with retaining the nanotube morphology (Figures 1D,E). According to this result, the optimal deposition of ZrO_2 nanoparticles did not alter the characteristics of the NTs. However, this deposition led to enhanced light scattering at the nanotubes, which will be discussed below, increasing the optical path of solar photons and enhancing light absorption. Figure 1F shows the corresponding EDS spectrum, revealing the existence of Ti, O, and Zr in the ZrO_2/TNTs.

Figure 2 shows HR-TEM images of the TNT/ZrO_2 photoanodes. The TEM photographs in Figure 2A,B indicate the uniformity and arrangement of the fabricated NTs morphology in the TNT/ZrO_2 films. The obtained TNTs were highly uniform, with an outer diameter of 170 ± 2 nm and a 30 ± 2 nm wall thickness. Further, the distinctive lattice fringes of 0.352 nm witnessed in the HR-TEM photograph in Figure 2C agree to the (101) plane of anatase TiO_2 (JCPDS no. 21-1272), signifying the anatase phase of the TNTs. The TNTs/ZrO_2 films were described by the existence of highly crystalline particles (6-10 nm), with an interplanar distance of 0.31 nm (Figure 2D), agreeing to the (111) reflection of monoclinic ZrO_2 (JCPDS Number 1309-37-1). EDS confirmed the presence of Zr in these NTs (Figures 1F and S1), indicating that although Zr could probably replace Ti in the anatase-TNTs lattice, as revealed by the diffraction pattern, a significant fraction of Zr was present in the monoclinic-ZrO_2 particles on the surface of NTs. The creation of ZrO_2 particles upon Zr incorporation has been demonstrated even for lower doping densities (<1 at.%) under high temperature and pressure sintering conditions.[38]

Structural and optical investigations were conducted to examine the role of incorporating ZrO_2 nanoparticles into the TNTs on the PEC features. First, an XRD analysis of TNTs decorated with different Zr loadings was performed (Figure S2). First, the remarkable shift of the (101) anatase peak at approximately 25.6° to the right at the minimum Zr loading of 2 mC, indicating a slight reduction in the lattice volume, can be related to the extended annealing step at 450°C after Zr loading, as TNTs have complicated annealing behavior.[46,47] Interestingly, increasing the Zr loading systematically increased the lattice constant, which is consistent with the bigger Zr^{4+} ion. The annealing step could, therefore, facilitate the addition of Zr into the TiO_2 lattice. The larger ionic radius of Zr^{4+} related to that of Ti^{4+} results in lattice strain. In order to alleviate this strain, surface oxygen can escape the lattice. This can result in both reductions and leave a hole trap behind, thus improving the photocatalytic activity.[48,49] Thus, adding Zr^{4+} in the TiO_2 lattice can result in lattice defects that can work as traps for charge carriers, extending the absorption range.[48] A

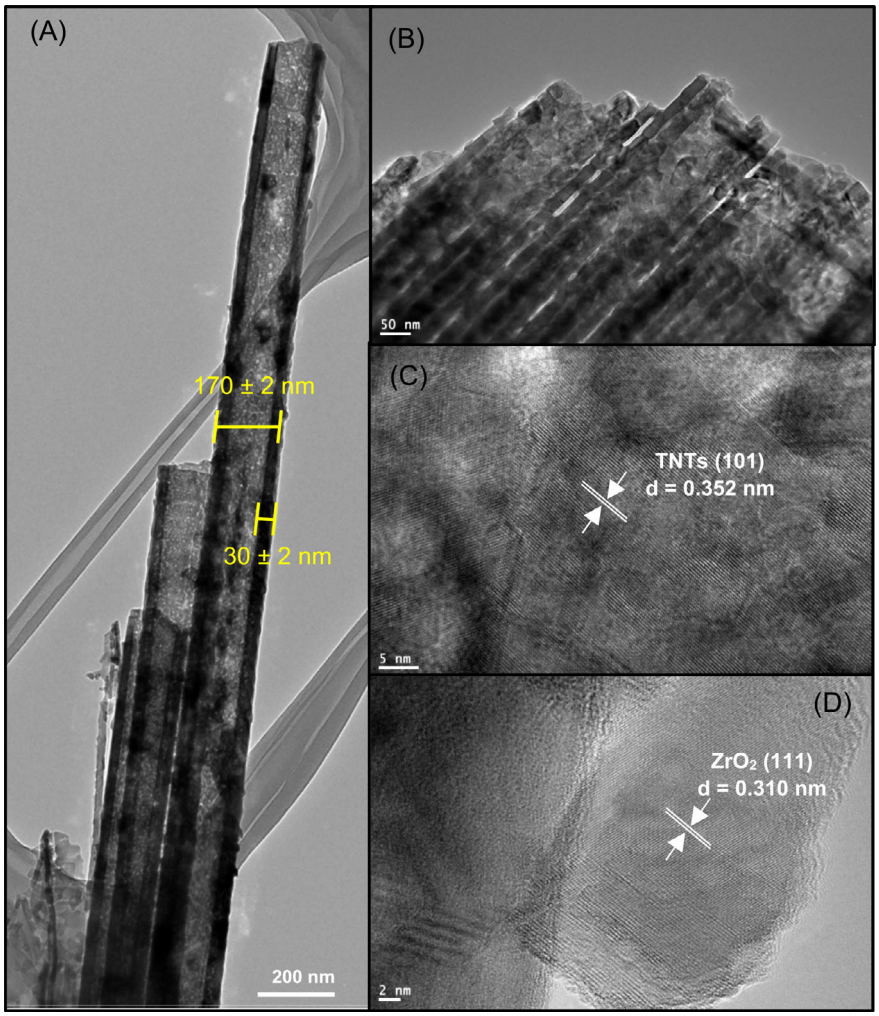

FIGURE 2 (A) HR-TEM micrograph displaying the high uniformity and reproducibility of the second anodized TiO_2 nanotubes (TNTs)/ZrO_2 films; (B,C) at a different magnification of TNTs/ZrO_2; (D) TEM micrograph of the ZrO_2 nanoparticles over TNTs

three-electrode current-voltage (J-V) analysis was executed for PEC tests under AM1.5G conditions in 0.1 M PBS (Figure S3**)**. These results confirmed that the optimized electrodeposited charge was 2 mC/cm^2.

3.2 | Microstructure and physicochemical properties of TNTs/ZrO_2/CoPi arrays

DRS was engaged in defining the optical bandgap, and absorption features of bare TNTs, TNTs/ZrO_2, and TNTs/ZrO_2/CoPi composite substrates; the obtained spectra are displayed in Figure 3A,B. Figure 3A displays that both ZrO_2 and CoPi depositions enhanced the overall absorption profiles, which can be credited to useful enhanced light scattering caused by the deposited films[45] in addition to defect-stimulated absorption.[48-50] The TNTs/ZrO_2 film spectrum exhibited a slight blue shift in the absorption edge, that is, to a higher bandgap, as the ZrO_2 nanoparticles were decorated over onto the TNT arrays. The bare TNT array spectrum indicated absorption at wavelengths up to 400 nm, agreeing to a bandgap of 3.16 eV, consistent with previously reported values for TiO_2.[51,52] The calculated bandgap of the films indicated that the introduction of CoPi and ZrO_2 nanoparticles does not have a significant effect on the absorption onset; however, their effect is mainly enhancing the overall absorption, which improved the PEC performance.

The crystal structures of the fabricated films were studied using XRD. Figure 3C presents XRD patterns recorded at room temperature for the TNT arrays before and after incorporating ZrO_2 and/or CoPi films. As shown, the anatase TiO_2 phase (JCPDS card no: 21-1272) and the metallic Ti phase (JCPDS file no: 44-1294) were clearly detected for TNT films on the Ti foil.[45] No diffraction peaks corresponding to the ZrO_2 crystalline phase were observed in the diffraction patterns of the TNTs/ZrO_2 films. Despite the existence of ZrO_2 nanoparticles on the TNTs surface, the absence of ZrO_2 XRD peaks can be explained by the small ZrO_2 nanoparticles' loading, in addition to their small grain size, that is below the XRD detection limit. There were also no diffraction peaks corresponding to CoPi in the pattern of a triple-layered

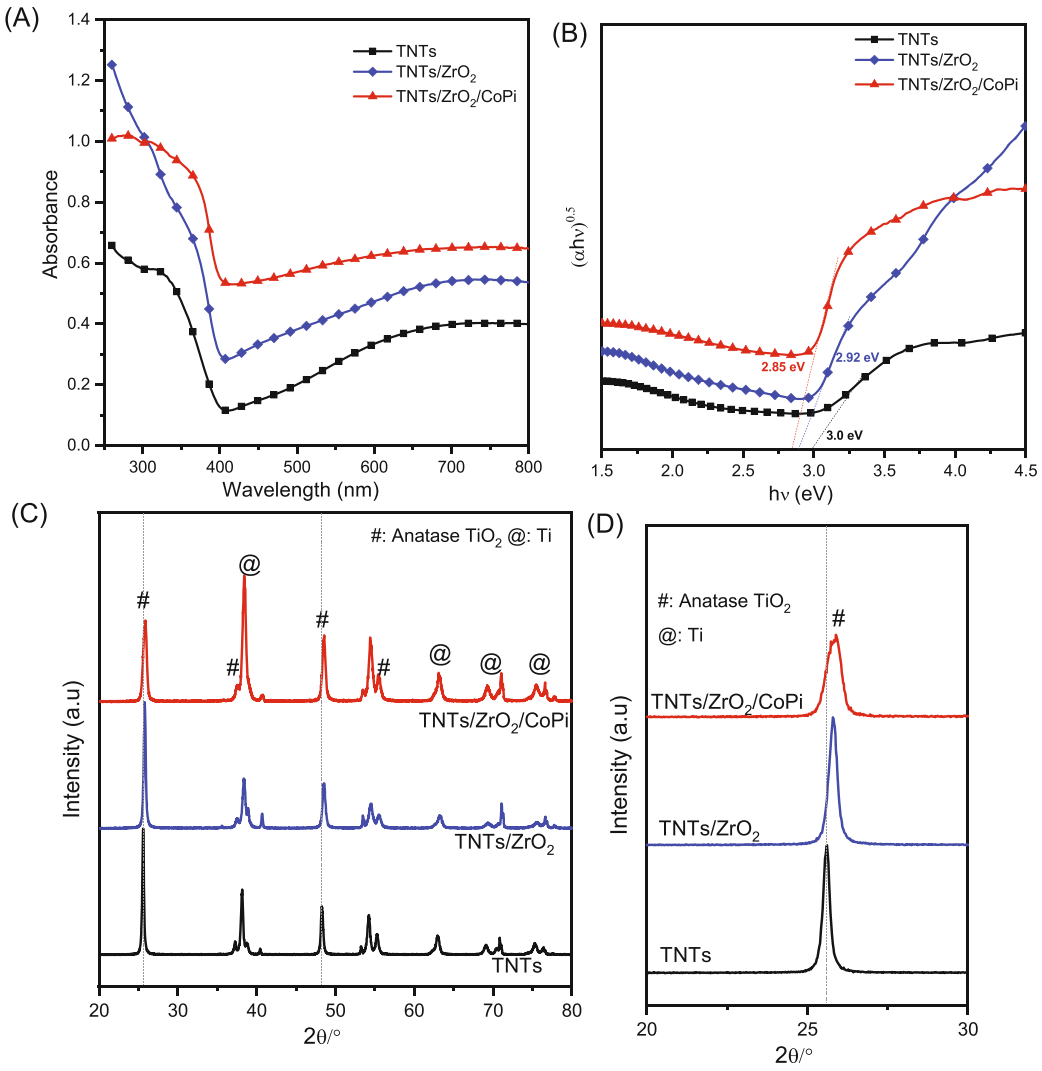

FIGURE 3 (A) UV-vis absorption spectra of the TiO_2 nanotube (TNT) array, TNTs/ZrO_2, and CoPi/ZrO_2/TNTs on FTO substrates. (B) Tauc plot displaying the relationship of $(\alpha hv)^{1/2}$ vs E (eV) with a bandgap of 3.0 eV for TNTs, 2.92 eV for TNTs/ZrO_2, and 2.85 eV for TNTs/ZrO_2/CoPi. (C) X-ray diffraction patterns for the TNT array, TNTs/ZrO_2, and TNTs/ZrO_2/CoPi films

TNTs/ZrO_2/CoPi sample. This is mainly due to the amorphous nature of CoPi in addition to the relatively small CoPi loading ensured by the photoassisted electrodeposition method.[11,53]

Figure 4 displays the surface morphology of the TNTs/ZrO_2/CoPi composite films. The photoassisted electrodeposition of CoPi onto the TNTs (Figure 4A,C) could fairly retain the open-top and continuous NT morphology, keeping a reachable surface area and allowing the rapid permeation of electrolyte ions. Figure 4B presents a cross-sectional micrograph of the TNTs/ZrO_2/CoPi composite film. As shown, the TNT array was well-arranged, and the tube diameter and tube wall thickness did not change after incorporating CoPi over the TNTs. However, after introducing CoPi, some TiO_2 was distributed as nanofibers on the TNTs surface (Figure 4C). This can substantially enhance the light scattering effects at the nanotube surface, probably explaining the enhanced sub-bandgap absorption spectrum. An EDS analysis determined the metal doping levels in the fabricated electrodes. Figure 4D shows the EDS spectrum, in which Co, P, Zr, Ti, and O signals are detected, confirming the introduction of the CoPi layer. The CoPi coatings were further investigated via EDS mapping analysis, as presented in Figure S4. The mapping results clearly show that the CoPi layer uniformly coated the TNTs/ZrO_2 semiconductor surface.

XPS performed a detailed surface analysis of the triple-layered TNTs/ZrO2/CoPi photoanodes, and are presented in Figure S5. The survey spectrum specified the attendance of Ti, O, Zr, Co, and P (Figure S5A). The Ti 2p high-resolution spectra for the TNTs/ZrO_2/CoPi composite films are presented in Figure S5B. XPS peaks corresponding to Ti $2p_{1/2}$ and $2p_{3/2}$ were observed at

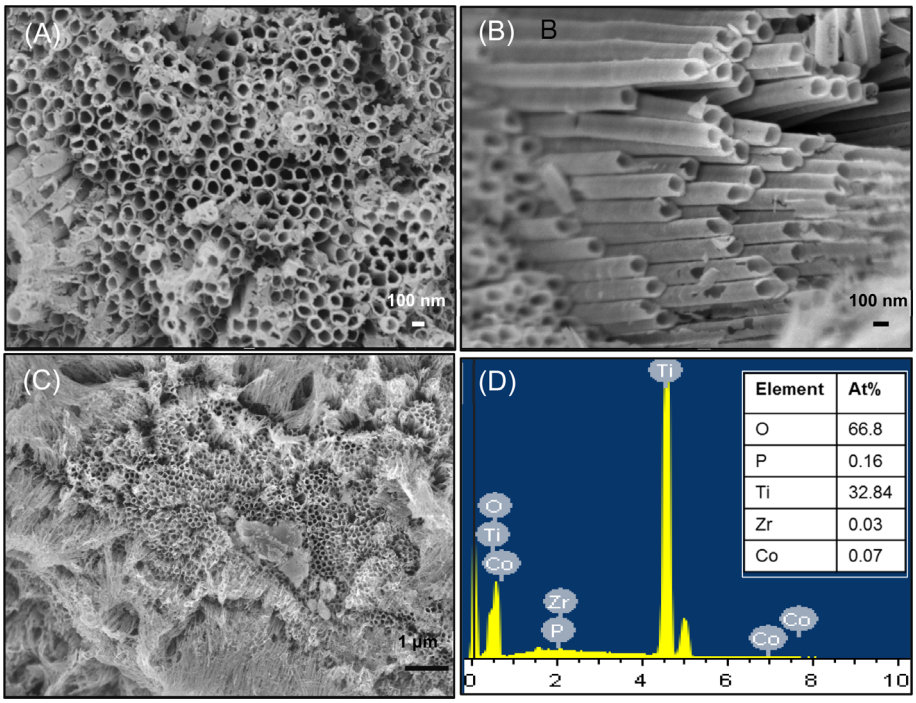

FIGURE 4 (A) A top-view and (B) cross-sectional SEM image of TNTs/ZrO_2/CoPi film. (C) A top-view SEM image with a low magnification. (D) energy-dispersive X-ray spectrometers results for TNTs, Zr, Co, and P

465 and 459.4 eV, correspondingly, indicating the 4+ state of Ti related to TNTs (Figure S5B). The existence of O^{2-} ions bound with Ti^{4+}, Zr^{4+}, and Co^{3+} to form the related oxide compounds is indicated by the presence of peaks at 530.6 eV inside the complex band connected with the O 1 s orbital (Figure S5C). The existence of Zr over the doped electrodes is further demonstrated by the occurrence of two peaks positioned at 187.3 eV (Zr $3d_{3/2}$) and 182.1 eV (Zr $3d_{5/2}$), indicating the 4+ state typical of ZrO_2 (Figure S4D). Interestingly, in the case of Co 2p spectrum (Figure S5E), cobalt ions could not be detected or remained below the detection limit. The quantity of Co was assessed to be <0.1 at. % for best optimized TNTs/Zr/CoPi, which is below the instrument's detection limit. As seen in Figure S5F, the BE of P 2p is at approximately 135.2 eV, representing P in the phosphate group, endorsing that P subsists as the nature of the phosphate group.[39]

3.3 | PEC properties of TNTs/ZrO_2/CoPi arrays

To assess the PEC features for solar-light-driven conversion, the fabricated TNTs, TNTs/ZrO_2, and TNTs/ZrO_2/CoPi composite electrodes were studied under constant (Figure 5A) and chopped (Figure 5B) irradiation in a 0.1 M PBS (pH of 7.5) solution. As demonstrated in Figure 5A, the parent TNT arrays displayed a photocurrent density of 0.26 mA/cm^2 at 1.23 V_{RHE}, and the photocurrent for TNTs/ZrO_2 was significantly enhanced. Compared with the parent TNT films, the composite TNTs/ZrO_2/CoPi electrodes revealed a photocurrent density of 0.86 mA/cm^2 at 1.23 V_{RHE}, which was more than a 4-fold improvement. This was accompanied by a significant cathodic change in the onset potential (350 mV). Comparatively, a photoanode with only CoPi loaded on bare TNTs under identical conditions was fabricated (Figure S6), and the results indicate that the CoPi coating alone had only lesser PEC activity. Further, Figure 5B shows the LSV plots for all the fabricated electrodes subjected to repeated light on/off cycles. These investigations indicated that incorporating the compound CoPi/ZrO_2 layer was a major factor in enhancing PEC water oxidation activity. The attained photocurrent in the J-V curve of the TNTs/ZrO_2/CoPi composite film under chopped illumination was almost linear and was reached rapidly upon switching the light on. This observed ideal performance is identical to that previously reported for CoPi-incorporated Fe_2O_3 electrodes.[54]

LSV plots of TNTs/ZrO_2 were also obtained by employing Na_2SO_3 as an efficient hole scavenger, and the PEC performance under repeated on/off cycles is presented in Figure 5C. As shown, with the support of Na_2SO_3, the TNTs/ZrO_2 exhibited a noteworthy enhancement in onset potential (0.145 V) and the photocurrent density (0.82 mA/cm^2). Importantly, these parameters reveal the enhanced PEC features of the CoPi-loaded TNTs/ZrO_2 samples, except in the lower bias region. Figure 5D summarizes the photocurrent densities of the investigated samples at 1.23 V_{RHE}. According to these comparisons, under AM 1.5G, incorporating ZrO_2 and

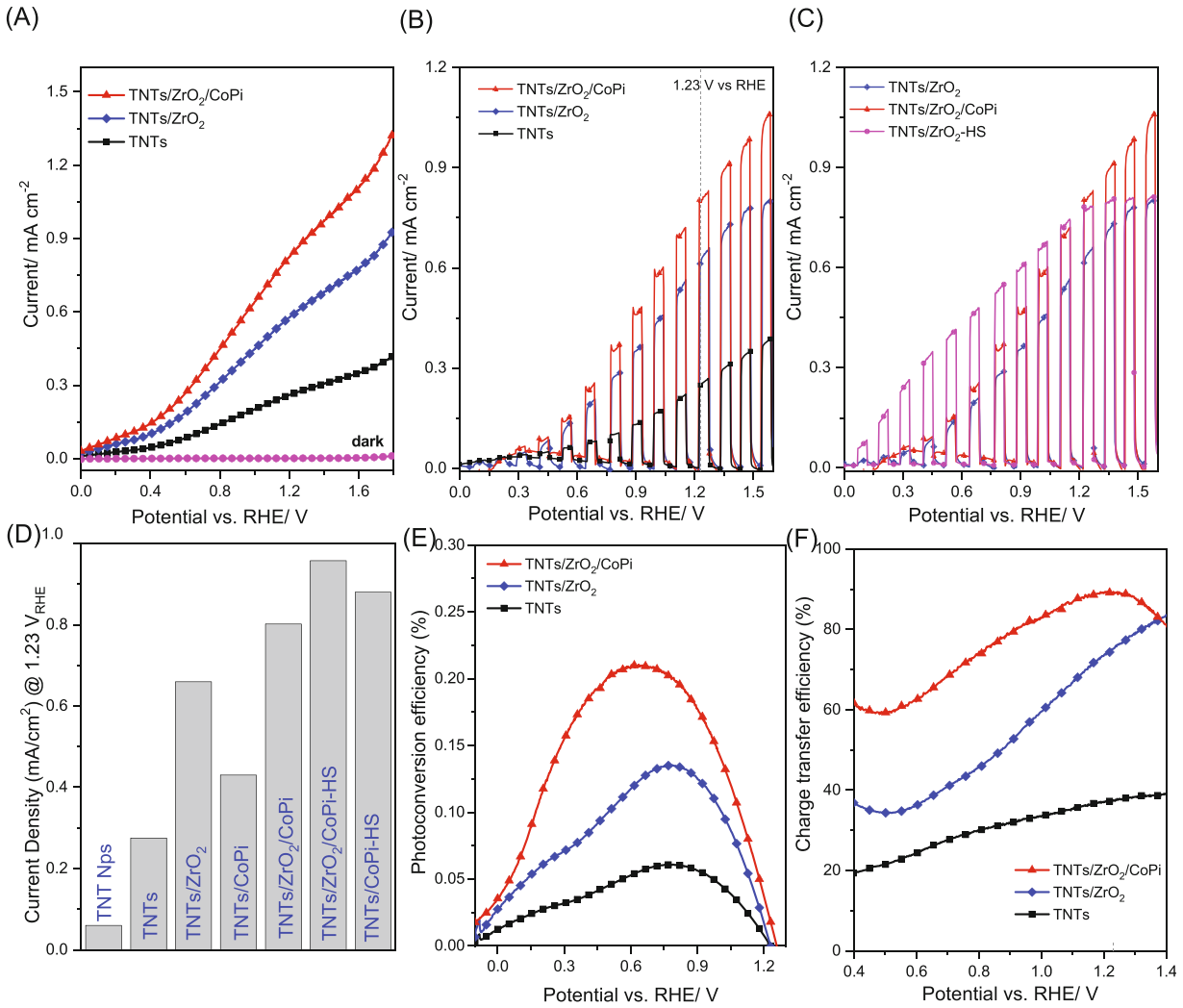

FIGURE 5 (A) LSVs characteristics for bare TiO_2 nanotubes (TNTs), TNTs/ZrO_2 (Zr molar concentration 2.5% with optimum charges equal 2 mC), TNTs/ZrO_2/CoPi (CoPi deposited on TNTs/ZrO_2 array by photo-assisted electrodeposition) evaluated in 0.1 M PBS (pH 7.5) under incessant illumination circumstances. (B) Photocurrent-potential characteristics under chopped illumination conditions for all investigated photoanodes (C) changes in photocurrent for all fabricated electrodes in the absent and present 1 M Na_2SO_3 as a hole scavenger. (D) Comparative plots for all photoanodes at 1.23 V_{RHE}. (E) photoconversion efficiency and (F) charge transfer efficiency of all photoanodes

the CoPi layer was essential for improving the PEC features to increase efficiency and stability. Figure 5E presents plots of the PCE vs the applied bias for the fabricated bare TNTs, TNTs/ZrO_2, and TNTs/ZrO_2/CoPi composite films. The bare TNTs revealed a maximal PCE of 0.06% at 0.76 V_{RHE}. With the incorporation of ZrO_2, the efficiency increased to 0.13% at 0.76 V_{RHE}. For the TNTs/ZrO_2/CoPi photoanodes, the PCE has a maximum of 0.21% at a lower bias of 0.66 V_{RHE}, which was a nearly 3.5-fold enhancement compared with that for the bare TNTs.

The enriched PEC performance of the TNTs/ZrO_2/CoPi catalysts was further assessed by examining the charge-transfer efficiencies (η_{CT}), and the results are presented in Figure 5F. The TNT photoanodes yielded only <37% η_{CT}, even at an applied potential as high as 1.23 V_{RHE} (at which the larger electric field generated by the bias hampers surface recombination processes). After incorporating ZrO_2, the η_{CT} of the TNTs/ZrO_2 photoanode was improved to approximately 75% at 1.23 V_{RHE}, indicating accelerated charge transfer kinetics. For the TNTs/ZrO_2/CoPi composite photoanodes, the η_{CT} reached 90%. These investigations revealed that incorporating CoPi into the TNTs/ZrO_2 created an efficient interface with water. The deposition of both ZrO_2 and CoPi layers could significantly promote better charge transfer kinetics in the fabricated system by enhancing the conductivity and carrier-separation efficiency of the TNT photoanodes, as will be discussed below.

Investigation of the wavelength-dependent PEC features of the modified TNTs was also performed to recognize the synergistic effects of CoPi and ZrO_2 on the PEC

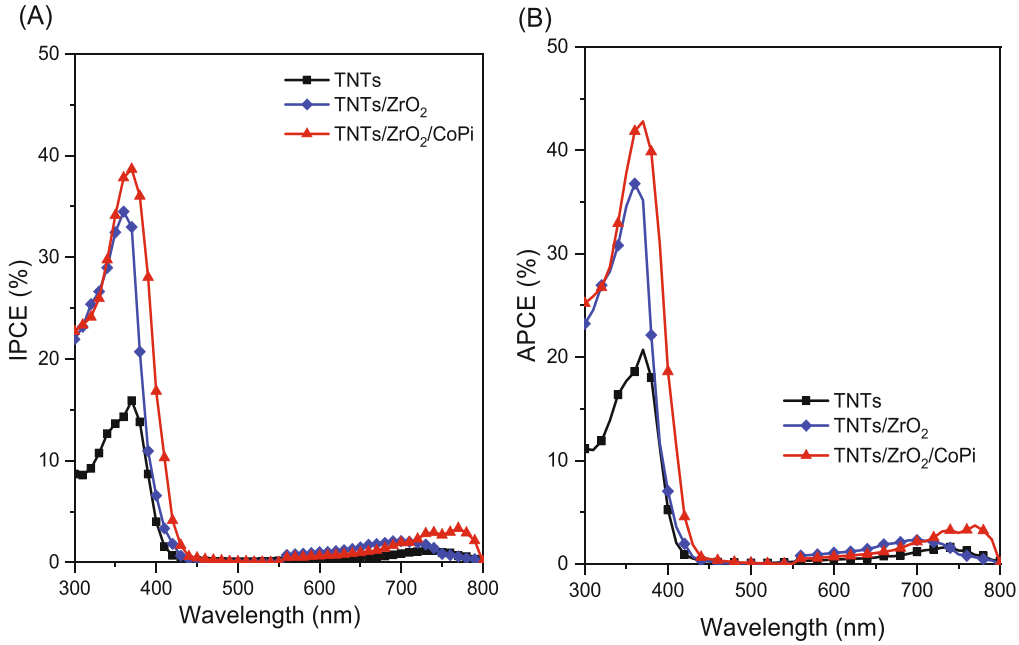

FIGURE 6 (A) Incident photon-to-current efficiency and (B) absorbed photon-to-current efficiency spectra of the TiO_2 nanotubes (TNT), TNTs/ZrO_2, and TNTs/ZrO_2/CoPi photoanodes assessed at an applied bias of 1.23 V_{RHE} in 0.1 M PBS (pH of 7.5)

features and the light absorption of the electrodes. Figure 6A and B presents the IPCE and ACPE data. The IPCE spectra of the TNTs/ZrO_2/CoPi composite arrays were related to the TNTs/ZrO_2 and TNTs at 1.23 V employing a monochromator (Figure 6A). After the CoPi co-catalyst loading, the TNTs/ZrO_2/CoPi composite sample exhibited significantly enhanced IPCE and APCE values than the bare TNTs and TNTs/ZrO_2. Further, the onset of the IPCE spectra was, respectively, at 440 and 420 nm for the TNTs/ZrO_2/CoPi and TNT photoelectrodes. For the TNTs, TNTs/ZrO_2, and TNTs/ZrO_2/CoPi, the IPCE at 420 nm was 0.65%, 1.85%, and 4.14%, respectively. The IPCE value was the highest for TNTs/ZrO_2/CoPi, indicating that more light can be absorbed by the composite photoanodes and can create holes to oxidize water molecules at the interface. The APCE spectra of the samples were also evaluated (Figure 6B), and the values were somewhat higher than those of the associated IPCE, indicating that the majority of the photo-generated charge carriers were efficiently extracted for PEC water oxidation.

To summarize, the preceding results elucidate the synergistic effects of ZrO_2 and CoPi deposition on the PEC features of the TNTs. From the above thorough measurements on the electrode materials and performance, we can attribute the observed enhancement to both ZrO_2 and CoPi. First, as confirmed by XRD and HRTEM measurements, the post-annealing treatment after Zr deposition resulted in two outcomes: Zr doping in the TNT bulk as well as oxidized Zr (ie, ZrO_2) nanoparticles on the nanotube surface. The Zr doping in bulk is evident from the systematic XRD peak shift with increasing Zr loading (Figure S2). Zr bulk doping can have desirable effects by increasing the number of traps for charge carriers, thus prolonging their lifetime. In addition to that, Zr^{4+} doping results in lattice strain enhancement/relief bulk/surface process that can ultimately result in surface oxygen vacancies, which also increases the photoelectrode efficiency.[48,49] As clearly observed in HRTEM and SEM images, not all Zr diffused by annealing into the TNT lattice and ZrO_2 nanoparticles were also attached to the nanotube surface, scattering by which could explain, at least partially, the enhanced light absorption in the visible region for the Zr-coated samples.[45,49] The synergistic effect of both layers could result in a large boost in both photocurrent as well as onset potential of the TNTs-based electrode.

To examine the charge-carrier mobility and PEC water-oxidation kinetics of the fabricated composite photoanodes, EIS was performed at 1.0 V_{RHE} under continuous illumination (Figure 7A). TNTs/ZrO_2/CoPi had the smallest arc radius among all the photoanodes, indicating that the synergistic incorporation of ZrO_2 and CoPi reduced the charge-transfer resistance and stimulated the charge transport in the TNTs photoanodes.[55,56] For the composite photoanodes, the incorporation of CoPi promoted the charge separation at the bulk electrode and enhanced the PEC water-splitting activity. CoPi- addition improved both the charge-carrier density and electronic conductivity, thereby reducing the

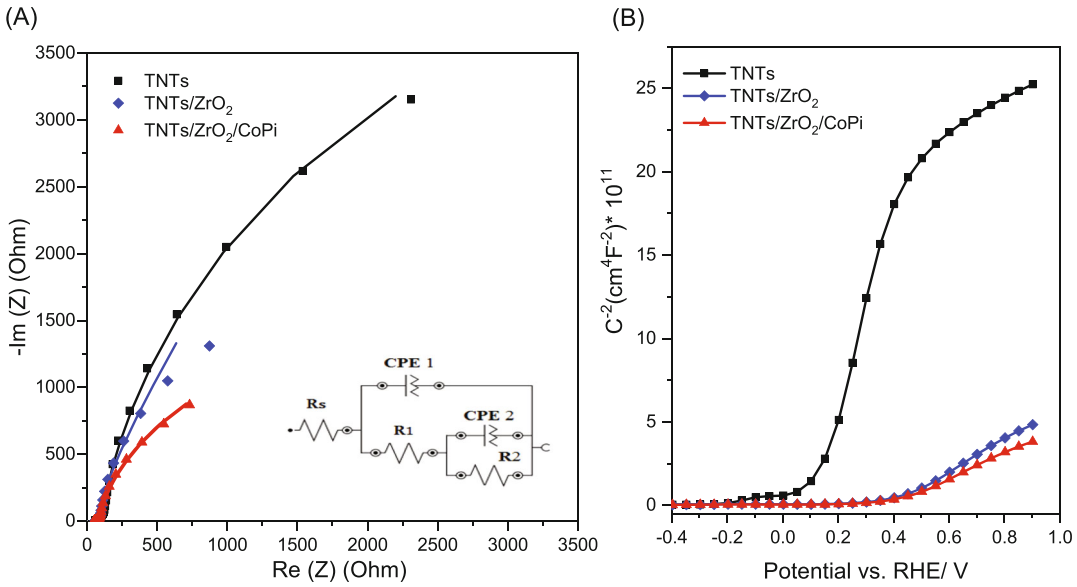

FIGURE 7 (A) Photoelectrochemical impedance spectroscopy results for TiO_2 nanotubes (TNTs)/ZrO_2/CoPi photoanodes compared with TNTs/ZrO_2 and bare TNT photoanodes (Nyquist plots) at 1.0 V_{RHE} with an alternating-current potential, in the frequency range of 100 kHz to 0.05 Hz. (B) Mott-Schottky plots for bare TNTs, TNTs/ZrO_2, and TNTs/ZrO_2/CoPi photoelectrodes in the dark at a fixed frequency of 100 Hz

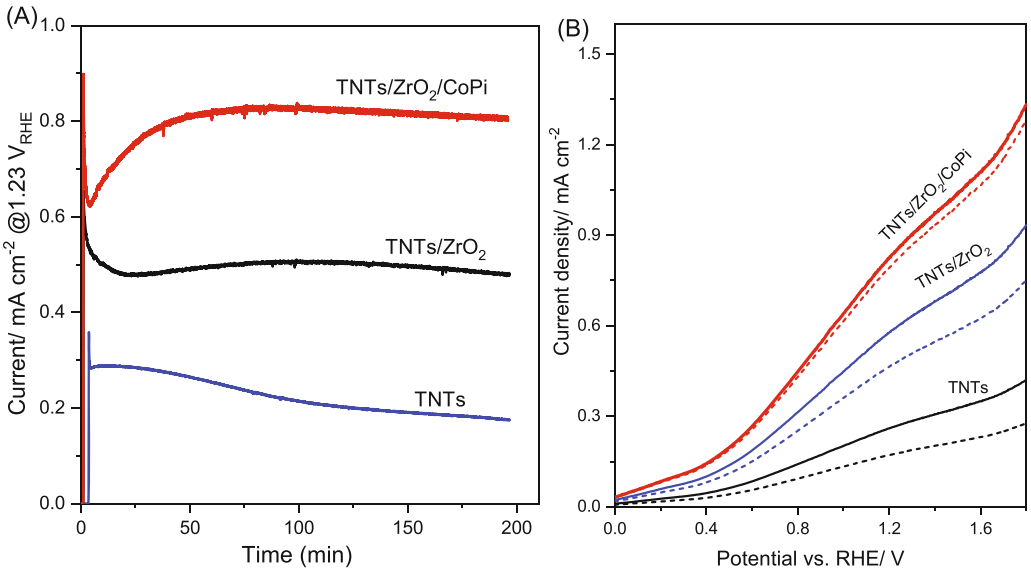

FIGURE 8 (A) J-t curves for the photostability of bare TiO_2 nanotubes (TNTs), TNTs/ZrO_2, and TNTs/ZrO_2/CoPi photoanodes in 0.1 M PBS (pH of 7.5) under illumination (AM 1.5G). (B) LSVs characteristics for bare TNTs, TNTs/ZrO_2, and TNTs/ZrO_2/CoPi photoanodes before (solid lines) and after (dotted lines) a 2-hour stability test

resistance (Table S1). In this regard, the CoPi incorporation improved the PEC features by improving the charge separation of carriers and water-splitting reaction on the electrode surface of the TNTs, which is identical to the previously reported behavior of TiO_2/CoPi[55] and $BiVO_4$/CoPi.[56]

As indicated by the Mott-Schottky plots in Figure 7B, all the fabricated TNT photoanodes were n-type semiconductors with a positive slope. The synergistic incorporation of ZrO_2 and CoPi induced a steady decrease in the slope from TNTs to TNTs/ZrO_2 and then to TNTs/ZrO_2/CoPi, suggesting an increased charge-carrier density.[57] When Zr^{4+} is substituted for Ti^{4+}, it acts as a recombination center in the TNT lattice.[49] Further, the efficient charge separation at the TNTs/ZrO_2/CoPi interface can efficiently extract the obtained holes

TABLE 1 Recent advances in different kinds of TiO_2 nanotubes (TNTs)-based photoelectrodes with co-catalysts and their photoelectrochemical features for water splitting reactions

S. No	Electrode	Electrolyte (pH)	Co-catalyst (synthesis, media and deposition time)	Light source	Current density (mA/cm^2)	References
1	TNTs nanowire/CoPi	0.1 M PBS (pH 7)	Co-Pi photo-assisted electrodeposition	100 mW/cm^2	≈ 0.46 at 1.23 V_{RHE}	58
2	N-modified TiO_2 nanowires ($TiO_{1.988}N_{0.012}$)	1.0 M KOH	Hydrothermal Co and Ag	100 mW/cm^2	≈ 0.6 for Co @ ≈ 0.46 for Ag @ 1.23 V_{RHE}	59
3	TiO_2/CdS/Co-Pi Nanowire Array	0.1 M KPi buffer (pH 7)	Co-Pi photoassisted electrodeposition	AM 1.5 100 mW/cm^2	≈ 0.4 @ 1.23 V_{RHE}	60
4	CoPi/nanocrystalline TiO_2 (nc-TiO_2)	0.5 M $NaClO_4$	Co-Pi (photoassisted electrodeposition)	AM 1.5 100 mW/cm^2	170 μA/cm^2 at 0.6 V vs Ag/AgCl, 90 μA/cm^2 TiO_2 alone	61
5	TiO_2 NTs/ZrO_2	1. 0.1 M PBS (pH 7.5)	Vacuum annealing	AM 1.5 100 mW/cm^2	0.72 @1.23 V_{RHE}	45
6	$NiFeOH_x/TiO_2$	1.0 M KOH (pH 13.6)	Electrodeposition	AM 1.5 100 mW/cm^2	0.2 @1.23 V_{RHE}	62
7	B,N-co doped TNTA	0.1 M Na_2SO_4	Electrochemical treatment	AM 1.5 100 mW/cm^2	0.57 @1.23 V_{RHE}	63
8	WO_3/TiO_2 NTs	1.0 M KOH	Anodization method	AM 1.5 100 mW/cm^2	0.62 @ 0.2 $V_{Ag/AgCl}$	64
9	Hydrogenated TiO_2 NTs	1.0 M NaOH/1 wt % of EG	Electrochemical treatment	AM 1.5 100 mW/cm^2	0.65 @ 0 $V_{Ag/AgCl}$	65
10	B-TiO_2/Al_2O_3	0.1 M Na_2SO_4	electrodeposition	AM 1.5 100 mW/cm^2	1.2 @ 1.23 V_{RHE}	66
11	Reduced TiO_2 NTAs	1 M NaOH	Chemical method	370 mW/cm^2 ($\lambda > 400$ nm)	0.73 @ 1.23 V_{RHE}	67
12	Ta/TNTs	1 M KOH	Electrochemical treatment	AM 1.5 100 mW/cm^2	0.5 @0.2 $V_{Ag/AgCl}$	68
13	Ag_2S/TiO_2 NTAs	0.5 M Na_2S	sequential-chemical bath deposition	25 mW/cm^2 ($\lambda > 385$ nm)	0.84 @ 0 $V_{Ag/AgCl}$	69
14	TNTs/ZrO_2/CoPi Electrodeposition	0.1 M NaPi buffer pH (7.5)	Co-Pi photo-assisted electrodeposition	AM 1.5 100 mW/cm^2	≈ 0.86 mA/cm^2 at 1.23 V vs RHE	This work

allowing them to be transported to the CoPi layer, contributing to faster PEC water-oxidation reactions rather than accumulating on the TNTs surface, which relieved the charge accumulation at the electrode/electrolyte interfaces.

Photocatalytic durability is essential for the long-term application of the TNTs/ZrO_2/CoPi composite electrodes in the PEC water-splitting system. Figure 8A presents the variation of the photocurrents with respect to time at a continuously applied bias of 1.23 V in a PBS solution under constant illumination. As explained in Figure 8A, the TNTs modified with the ZrO_2/CoPi co-catalyst exhibited an enhanced photocurrent and reached solar-induced water oxidation with a photocurrent density of 0.86 mA/cm^2 was nearly a 5-fold enhancement than that of parent TNTs. Notably, the TNTs/ZrO_2/CoPi composite photoanodes exhibited reasonably good durability, with <10% photocurrent loss in 2 hours. The PEC performance was evaluated after a stability test to examine the mass loss of the fabricated photoanodes, and the results are shown in Figure 8B. The LSV plots of the TNTs/ZrO_2/CoPi composite electrodes acquired after 2 hours revealed no detectable changes than the bare TNTs (Figure 8B). Table 1 compares the photocatalysts fabricated in the present study with previously reported photocatalysts. The results indicate that our TNTs/ZrO_2/CoPi composite photoanodes are stable and effective for oxidizing water into O_2. All the obtained results suggest that the co-catalytic influence of ZrO_2 and CoPi decoration significantly improved the PEC features and durability of TNT photoanodes by enhancing the charge-carrier density and the surface oxidation kinetics.

PEC production of oxygen evolution via photoelectrocatalysis at TiO_2/ZrO_2/CoPi composite photoanodes was observed via an Oxysense instrument. Figure S7A evidences the oxygen evolution concentration with respect to the time for TiO_2/ZrO_2/CoPi composite photoanodes at 0.6 V_{RHE} and with incessant irradiation conditions. After CoPi introduction, visible-light photons ($\lambda > 420$ nm) urged dioxygen evolution over the surface of TiO_2/ZrO_2/CoPi photoanodes, and their corresponding photocurrent measurements are displayed in Figure S7B. With the assistance of potential (0.6 V vs RHE), dioxygen generation was sensed, and their concentrations were likely to surge linearly with time intervals. Conversely, the fabricated TiO_2/ZrO_2/CoPi photoanodes evidenced considerable durability toward the continuous irradiation (Figure S7B).

Based on the earlier PEC examinations, a probable PEC splitting mechanism of TNTs/ZrO_2/CoPi was proposed in Figure 9. The CoPi catalysts were loaded over the surface of and inside the ZrO_2 decorated TNTs. In the case of TNTs/ZrO_2 interface, where Zr-incorporation assisting the formation of defects in TNTs has been stated

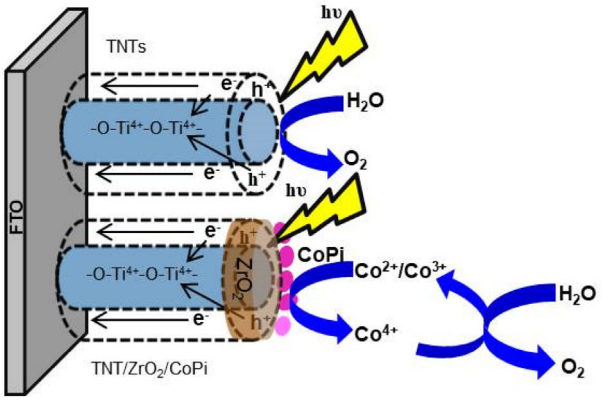

FIGURE 9 Schematic demonstration of charge transfer pathways in fabricated TiO_2 nanotubes (TNTs) and TNTs/ZrO_2/CoPi electrodes

to assist electron trapping over Zr^{4+} rather than on Ti^{4+} leads to suppressed charge recombination and successively advancing charge transfer kinetics and later PEC features for water oxidation. Further, the PEC performance is boosted by CoPi species. After alteration on the surface of the TNTs with ZrO_2 and CoPi, photogenerated holes will be quickly trapped by CoPi-WOC to oxidize OH^- to O_2 the electrons can reach the Pt to reduce water under the external bias. Additionally, the Mott-Schottky results showed a significant difference after ZrO_2/CoPi incorporation over TNTs, thereby enhancing the charge separation efficiencies remarkably. The CoPi-WOC, as a greatly effective catalytic material for oxygen evolution reaction, boosted the hole-trapping features to quicken the separation of photo-induced carriers. Benefiting from the Zr-doping and self-circulation of CoPi, at this beneficial condition, charge carriers are well separated and have sufficient time for water oxidation which enhances the PEC performance of the TNTs/ZrO_2/CoPi than bare-TNTs films. These results contribute to the understanding and designing effective PEC cells for solar fuel production.

4 | CONCLUSIONS

We demonstrated the synergetic catalytic effect of ZrO_2 doping and CoPi deposition over the surface of TNTs for PEC water splitting. These triple-layered TNTs/ZrO_2/CoPi photoanodes exhibited high PEC performance, particularly in the low-potential region, nearly 4-fold enhancements in the photoconversion efficiency compared with bare TNTs. Significantly, the PEC stability of the TNTs/ZrO_2 electrodes was improved after the incorporation of CoPi; approximately 90% of the initial photocurrent was retained after 2 hours of irradiation. EIS

revealed that the charge transfers at the photoanode/electrolyte interfaces were accelerated by enhanced carrier mobility and reduced charge-carrier surface recombination. These observed findings revealed an efficient approach via designing innovative catalytic materials based on rare-earth materials for photoelectrochemical and photocatalytic uses.

AUTHOR CONTRIBUTION

Maged N. Shaddad: Data curation, Formal analysis, Investigation, Writing - original draft. Prabhakarn Arunachalam: Conceptualization, Data curation, Formal analysis, Investigation, Supervision. Writing - review & editing. Mabrook S Amer: Data Curation Investigation. Mohmoud Hezam: Investigation. Haneen Abdullah Nasser AlOraij: Formal analysis; Sixto Gimenez: Supervision: Abdullah M. Al-Mayouf: Supervision, Project administration.

ACKNOWLEDGMENTS

This project was funded by the National Plan for Science, Technology, and Innovation (MAARIFAH), King Abdulaziz City for Science and Technology, Kingdom of Saudi Arabia, Award Number (3-17-02-001-0011).

CONFLICT OF INTEREST

The authors declare that they have no known competing financial interests or personal relationships that could have appeared to influence the work reported in this paper.

DATA AVAILABILITY STATEMENT

All data generated or analyzed during this study are included in this published article (and its Supporting Information files).

ORCID

Prabhakarn Arunachalam https://orcid.org/0000-0002-6293-1631

REFERENCES

1. Walter MG, Warren EL, McKone JR, et al. Solar water splitting cells. *Chem Rev*. 2010;110:6446-6473.
2. Fujishima A, Honda K. Electrochemical photolysis of water at a semiconductor electrode. *Nature*. 1972;238:37-38.
3. Shuya Z, Lu H, Xudong L, et al. Polydopamine and Nafion bilayer passivation modified CdS photoanode for photoelectrochemical hydrogen evolution. *Int J Energy Res.* 2022;46:4506-4515. doi:10.1002/er.7444
4. Roy P, Das C, Lee K, et al. Oxide nanotubes on Ti− Ru alloys: strongly enhanced and stable photoelectrochemical activity for water splitting. *J Am Chem Soc*. 2011;133:5629-5631.
5. Liu Z, Xu K, Yu H, Sun Z. Synergistic effect of ag/MoS2/TiO2 heterostructure arrays on enhancement of photoelectrochemical and photocatalytic performance. *Int J Energy Res*. 2021;45:6850-6862.
6. Nozik AJ. Photoelectrolysis of water using semiconducting TiO2 crystals. *Nature*. 1975;257:383-386.
7. Yang X, Wolcott A, Wang G, et al. Nitrogen-doped ZnO nanowire arrays for photoelectrochemical water splitting. *Nano Lett*. 2009;9:2331-2336.
8. Feng W, Lin L, Li H, Chi B, Pu J, Li J. Hydrogenated TiO2/ZnO heterojunction nanorod arrays with enhanced performance for photoelectrochemical water splitting. *Int J Hydrogen Energy*. 2017;42:3938-3946.
9. Kawasaki S, Nakatsuji K, Yoshinobu J, et al. Epitaxial Rh-doped SrTiO3 thin film photocathode for water splitting under visible light irradiation. *Appl Phys Lett*. 2012;101:033910-033912.
10. Smith RD, Prévot MS, Fagan RD, et al. Photochemical route for accessing amorphous metal oxide materials for water oxidation catalysis. *Science*. 2013;340:60-63.
11. Zhong DK, Cornuz M, Sivula K, Grätzel M, Gamelin DR. Photo-assisted electrodeposition of cobalt–phosphate (co–pi) catalyst on hematite photoanodes for solar water oxidation. *Energ Environ Sci*. 2011;4:1759-1764.
12. Lee MH, Park JH, Han HS, et al. Nanostructured Ti-doped hematite (α-Fe2O3) photoanodes for efficient photoelectrochemical water oxidation. *Int J Hydrogen Energy*. 2014;39:17501-17507.
13. Amer MS, Arunachalam P, Al-Mayouf AM, Prasad P, Alshalwi MN, Ghanem MA. Mesoporous tungsten trioxide photoanodes modified with nitrogen-doped carbon quantum dots for enhanced oxygen evolution photo-reaction. *Nanomaterials*. 2019;9:1502.
14. Arunachalam P, Nagai K, Amer MS, Ghanem MA, Ramalingam RJ, Al-Mayouf AM. Recent developments in the use of heterogeneous semiconductor photocatalyst based materials for a visible-light-induced water-splitting system—a brief review. *Catalysts*. 2021;11:160.
15. Yu SQ, Ling YH, Zhang J, Qin F, Zhang ZJ. Efficient photoelectrochemical water splitting and impedance analysis of WO3− x nanoflake electrodes. *Int J Hydrogen Energy*. 2017;42:20879-20887.
16. Liu M, de Leon SN, Park H. Water photolysis with a cross-linked titanium dioxide nanowire anode. *Chem Sci*. 2011;2:80-87.
17. Tang H, Prasad K, Sanjines R, Schmid PE, Levy F. Electrical and optical properties of TiO2 anatase thin films. *J Appl Phys*. 1994;75:2042-2047.
18. Takahashi M, Tsukigi K, Uchino T, Yoko T. Enhanced photocurrent in thin film TiO2 electrodes prepared by sol-gel method. *Thin Solid Films*. 2001;388:231-236.
19. Xia H, Xiong W, Lim CK, Yao Q, Wang Y, Xie J. Hierarchical TiO 2-B nanowire@ α-Fe2O3 nanothorn core-branch arrays as superior electrodes for lithium-ion microbatteries. *Nano Res*. 2014;7:1797-1808.
20. Chen X, Shen S, Guo L, Mao SS. Semiconductor-based photocatalytic hydrogen generation. *Chem Rev*. 2010;110:6503-6570.
21. Murphy AB, Barnes PR, Randeniya LK, et al. Efficiency of solar water splitting using semiconductor electrodes. *Int J Hydrogen Energy*. 2006;31:1999-2017.
22. Arunachalam P, Amer MS, Ghanem MA, Al-Mayouf AM, Zhao D. Activation effect of silver nanoparticles on the photoelectrochemical performance of mesoporous TiO2 nanospheres

photoanodes for water oxidation reaction. *Int J Hydrogen Energy*. 2017;42:11346-11355.
23. Hoyer P. Semiconductor nanotube formation by a two-step template process. *Adv Mater*. 1996;8:857-859.
24. Wang J, Lin Z. Dye-sensitized TiO_2 nanotube solar cells with markedly enhanced performance via rational surface engineering. *Chem Mater*. 2010;22:579-584.
25. Qin P, Paulose M, Dar MI, et al. Stable and efficient perovskite solar cells based on titania nanotube arrays. *Small*. 2015;11: 5533-5539.
26. Wang J, Zhao L, Lin VS, Lin Z. Formation of various TiO2 nanostructures from electrochemically anodized titanium. *J Mater Chem*. 2009;19:3682-3687.
27. Macak JM, Tsuchiya H, Ghicov A, et al. TiO2 nanotubes: self-organized electrochemical formation, properties and applications. *Curr Opin Solid State Mater Sci*. 2007;11:3-18.
28. Sang Y, Zhao Z, Tian J, et al. Enhanced photocatalytic property of reduced graphene oxide/TiO2 nanobelt surface heterostructures constructed by an in situ photochemical reduction method. *Small*. 2014;10:3775-3782.
29. Tian J, Hao P, Wei N, Cui H, Liu H. 3D Bi2MoO6 nanosheet/TiO2 nanobelt heterostructure: enhanced photocatalytic activities and photoelectochemistry performance. *ACS Catalysis*. 2015;5:4530-4536.
30. Varghese OK, Gong D, Paulose M, Ong KG, Grimes CA. Hydrogen sensing using titania nanotubes. *Sens Actuators B Chem*. 2003;93:338-344.
31. Shankar K, Mor GK, Prakasam HE, et al. Highly-ordered TiO2 nanotube arrays up to 220 μm in length: use in water photoelectrolysis and dye-sensitized solar cells. *Nanotechnology*. 2007;18:065707.
32. Song YY, Schmidt-Stein F, Bauer S, Schmuki P. Amphiphilic TiO2 nanotube arrays: an actively controllable drug delivery system. *J Am Chem Soc*. 2009;131:4230-4232.
33. Liu Q, Ding D, Ning C, Wang X. Cobalt-phosphate/Ni-doped TiO2 nanotubes composite photoanodes for solar water oxidation. *Mater Sci Eng B*. 2015;202:54-60.
34. Marschall R. Semiconductor composites: strategies for enhancing charge carrier separation to improve photocatalytic activity. *Adv Funct Mater*. 2014;24:2421-2440.
35. Ponja S, Sathasivam S, Chadwick N, et al. Aerosol assisted chemical vapour deposition of hydrophobic TiO2–SnO2 composite film with novel microstructure and enhanced photocatalytic activity. *J Mater Chem A*. 2013;1:6271-6278.
36. Lutterman DA, Surendranath Y, Nocera DG. A self-healing oxygen-evolving catalyst. *J Am Chem Soc*. 2009;131:3838-3839.
37. Arunachalam P, Al-Mayouf A, Ghanem MA, Shaddad MN, Weller MT. Photoelectrochemical oxidation of water using La (ta, Nb) O2N modified electrodes. *Int J Hydrogen Energy*. 2016; 41:11644-11652.
38. Rajeshwar K, de Tacconi NR, Chenthamarakshan CR. Semiconductor-based composite materials: preparation, properties, and performance. *Chem Mater*. 2001;13:2765-2782.
39. Kanan MW, Nocera DG. In situ formation of an oxygen-evolving catalyst in neutral water containing phosphate and Co2+. *Science*. 2008;321:1072-1075.
40. McDonald KJ, Choi KS. Photodeposition of co-based oxygen evolution catalysts on α-Fe2O3 photoanodes. *Chem Mater*. 2011;23:1686-1693.
41. Seabold JA, Choi KS. Effect of a cobalt-based oxygen evolution catalyst on the stability and the selectivity of photo-oxidation reactions of a WO3 photoanode. *Chem Mater*. 2011;23:1105-1112.
42. Arunachalam P, Shaddad MN, Ghanem MA, Al-Mayouf AM, Weller MT. Zinc tantalum Oxynitride (ZnTaO2N) photoanode modified with cobalt phosphate layers for the photoelectrochemical oxidation of alkali water. *Nanomaterials*. 2018; 8:48.
43. Kanan MW, Yano J, Surendranath Y, Dinca M, Yachandra VK, Nocera DG. Structure and valency of a cobalt− phosphate water oxidation catalyst determined by in situ X-ray spectroscopy. *J Am Chem Soc*. 2010;2010(132):13692-13701.
44. Shaddad MN, Ghanem MA, Al-Mayouf AM, Gimenez S, Bisquert J, Herraiz-Cardona I. Cooperative catalytic effect of ZrO2 and α-Fe2O3 nanoparticles on BiVO4 Photoanodes for enhanced Photoelectrochemical water splitting. *ChemSusChem*. 2016;9:2779-2783.
45. Shaddad MN, Cardenas-Morcoso D, García-Tecedor M, et al. TiO2 nanotubes for solar water splitting: vacuum annealing and Zr doping enhance water oxidation kinetics. *ACS Omega*. 2019;4:16095-16102.
46. Albu SP, Tsuchiya H, Fujimoto S, Schmuki P. TiO2 nanotubes–annealing effects on detailed morphology and structure. *Eur J Inorg Chem*. 2010;27:4351-4356.
47. Liu H, Liu G, Zhou Q. Preparation and characterization of Zr doped TiO2 nanotube arrays on the titanium sheet and their enhanced photocatalytic activity. *J Solid State Chem*. 2009;182: 3238-3242.
48. Lukáč J, Klementová M, Bezdička P, et al. Influence of Zr as TiO2 doping ion on photocatalytic degradation of 4-chlorophenol. *Appl Catal Environ*. 2007;74:83-91.
49. Chang SM, Doong RA. Characterization of Zr-doped TiO2 nanocrystals prepared by a nonhydrolytic sol− gel method at high temperatures. *J Phys Chem B*. 2006;110:20808-20814.
50. Hoffart L, Heider U, Jörissen L, Huggins RA, Witschel W. Transport properties of materials with the scheelite structure. *Solid State Ion*. 1994;72:195-198.
51. Xu M, Da P, Wu H, Zhao D, Zheng G. Controlled Sn-doping in TiO2 nanowire photoanodes with enhanced photoelectrochemical conversion. *Nano Lett*. 2012;12:1503-1508.
52. Wang X, Li Z, Shi J, Yu Y. One-dimensional titanium dioxide nanomaterials: nanowires, nanorods, and nanobelts. *Chem Rev*. 2014;114:9346-9384.
53. Zhong DK, Choi S, Gamelin DR. Near-complete suppression of surface recombination in solar photoelectrolysis by "co-pi" catalyst-modified W: BiVO4. *J Am Chem Soc*. 2011;133:18370-18377.
54. Klahr B, Gimenez S, Fabregat-Santiago F, Bisquert J, Hamann TW. Photoelectrochemical and impedance spectroscopic investigation of water oxidation with —Co–Pi-coated hematite electrodes. *J Am Chem Soc*. 2012;134:16693-16700.
55. Ai G, Mo R, Li H, Zhong J. Cobalt phosphate modified TiO2 nanowire arrays as co-catalysts for solar water splitting. *Nanoscale*. 2015;7:6722-6728.
56. Pilli SK, Furtak TE, Brown LD, Deutsch TG, Turner JA, Herring AM. Cobalt-phosphate (Co-Pi) catalyst modified Mo-doped BiVO 4 photoelectrodes for solar water oxidation. *Energ Environ Sci*. 2011;4:5028-5034.

57. Wang Y, Zhang YY, Tang J, et al. Simultaneous etching and doping of TiO2 nanowire arrays for enhanced photoelectrochemical performance. *ACS Nano*. 2013;7:9375-9383.
58. Ai G, Mo R, Li H, Zhong J. Cobalt phosphate modified TiO 2 nanowire arrays as co-catalysts for solar water splitting. *Nanoscale*. 2015;7:6722-6728.
59. Hoang S, Guo S, Hahn NT, Bard AJ, Mullins CB. Visible light driven photoelectrochemical water oxidation on nitrogen-modified TiO2 nanowires. *Nano Lett*. 2012;12:26-32.
60. Ai G, Li H, Liu S, Mo R, Zhong J. Solar water splitting by TiO2/CdS/Co–Pi nanowire array photoanode enhanced with co–pi as hole transfer relay and CdS as light absorber. *Adv Funct Mater*. 2015;25:5706-5713.
61. Liu D, Jing L, Luan P, Tang J, Fu H. Enhancement effects of cobalt phosphate modification on activity for photoelectrochemical water oxidation of TiO2 and mechanism insights. *ACS Appl Mater Interfaces*. 2013;5:4046-4052.
62. Xu Y, Ahmed R, Lin Q, Zangari G. (Photo) electrochemical water oxidation at anodic TiO2 nanotubes modified by electrodeposited NiFe oxy-hydroxides catalysts. *Electrochim Acta*. 2019;308:91-98.
63. Georgieva J, Valova E, Armyanov S, et al. A simple preparation method and characterization of B and N co-doped TiO2 nanotube arrays with enhanced photoelectrochemical performance. *Appl Surf Sci*. 2017;413:284-291.
64. Momeni MM, Ghayeb Y, Davarzadeh M. Single-step electrochemical anodization for synthesis of hierarchical WO3–TiO2 nanotube arrays on titanium foil as a good photoanode for water splitting with visible light. *J Electroanal Chem*. 2015;739:149-155.
65. Xu C, Song Y, Lu L, et al. Electrochemically hydrogenated TiO 2 nanotubes with improved photoelectrochemical water splitting performance. *Nanoscale Res Lett*. 2013;2013(8):1-7.
66. Liu C, Zhang C, Yin G, et al. A three-dimensional branched TiO2 Photoanode with an ultrathin Al2O3 passivation layer and a NiOOH Cocatalyst toward Photoelectrochemical water oxidation. *ACS Appl Mater Interfaces*. 2021;2021(13):13301-13310.
67. Kang Q, Cao J, Zhang Y, Liu L, Xu H, Ye J. Reduced TiO 2 nanotube arrays for photoelectrochemical water splitting. *J Mater Chem A*. 2013;1:5766-5774.
68. Altomare M, Lee K, Killian MS, Selli E, Schmuki P. Ta-doped TiO2 nanotubes for enhanced solar-light photoelectrochemical water splitting. *Chem A Eur J*. 2013;19:5841-5844.
69. Gholami M, Qorbani M, Moradlou O, Naseri N, Moshfegh AZ. Optimal Ag 2 S nanoparticle incorporated TiO 2 nanotube array for visible water splitting. *RSC Adv*. 2014;4:7838-7844.

SUPPORTING INFORMATION

Additional supporting information may be found in the online version of the article at the publisher's website.

How to cite this article: Shaddad MN, Arunachalam P, Amer MS, et al. Exploiting the synergistic catalytic effects of CoPi nanostructures on Zr-doped highly ordered TiO_2 nanotubes for efficient solar water oxidation. *Int J Energy Res*. 2022;46(9):12608-12622. doi:10.1002/er.8030